International Journal of Scientific Engineering and Applied Science (IJSEAS) – Volume-2, Issue-4,April 2016
ISSN: 2395-3470
www.ijseas.com

Influence of Temperature on Particulate Fracture of AA2024 Alloy/Titanium Oxide nanoparticulate Metal Matrix Composites

Chennakesava R Alavala
Department of mechanical Engineering, JNT University, Hyderabad, India

Abstract

The present work was to estimate thermoelastic behavior of AA2024 alloy/titanium oxide nanoparticle metal matrix composites. . The RVE models were employed to compute thermo-elastic behavior. The elastic moduli of AA2024 alloy/titanium oxide nanoparticle metal matrix composites decreased with the increase of temperature. The TiN nanoparticle was fractured due to heavy load transfer from AA2024 alloy and CTE mismatch.

Keywords: AA2024 alloy, titanium oxide, RVE model, thermoelastic, finite element analysis.

1. Introduction

Metal matrix composites with nanoparticulates have an enormous prospective for the use in automobile, aerospace, electronic and defense industries. [1, 2] Experimental studies indicated that the micro particles yielded the increasing strengthening and stiffening effects. For matrix materials, aluminum alloys are appreciated because of their low density and high ductility. However, they are deficient in strength and stiffness. For improvement of strength and stiffness in aluminum alloy based matrix materials, several reinforced particulates such as silicon carbide [3-5], alumina [6-8], alumina trihydrate [9], carbon [10], titnanium boride [11], silicon nitride [12], etc were exploited. The relevance of nanoparticle reinforced composites came very recently. Reinforcing of these nanoparticles into various metal matrices unlocked a key area of research in enhancing the properties of metal matrix composites.

The present work was to investigate thermoelastic behavior of AA2024 alloy/TiO_2 nanoparticulate metal matrix composites. Finite element analysis (FEA) was performed to evaluate thermoelastic behavior of metal matrix composites using representative volume element (RVE) relying on hydrostatic and isothermal loading.

2. Material and Methodology

The shear lag model [13] has been used to describe the build up and transfer of particle stress, σ_p from the point where the particle enters the matrix to some point along the particle axis where the tensile stress has decayed to zero. Failure of the particle/matrix interface occurs when the interfacial shear strength, τmax, is reached.

The shear lag distribution of strain, along a fully bonded particle can be described by [11, 12]

$$e_{app} = e_p \frac{\sinh[n(L_e - x/r)]}{\sinh(ns)} \quad (1)$$

where e_{app} is the strain acting on the particle outside the matrix, e_p is the particle strain at a distance x inside the matrix, L_e is the embedded length, r is the particle radius and s is the particle aspect ratio (L_e/r). The n parameter used in this paper is:

$$n^2 = \frac{2}{E_p E_m}\left[\frac{E_p V_p + E_m V_m}{V_m/(4G_p) + 1/(2G_m)\left((1/V_m)\ln(1/V_p) - 1 - (V_m/2)\right)}\right] \quad (2)$$

where E_p and G_P ate the particle elastic and shear moduli, E_m and G_m are the elastic and shear moduli of the matrix. V_p is the particle volume fraction and V_m is the volume fraction of matrix. The corresponding interfacial stress, τ at a distance x along the interface, is given by

$$\tau = \frac{n}{2} E_p e_{app} \frac{\cosh[n(L_e - x)/r]}{\sinh[ns]} \quad (3)$$

Is a maximum at the crack plane (x = 0). Since both the interfacial shear stress and the stress acting on the particle, are a maximum at the crack-plane then failure should be expected to initiate from this point. When x = 0, the Eq. (3) becomes:

$$\tau = \frac{n}{2} E_p e_p \quad (4)$$

If the particle deforms in an elastic manner (according to Hooke's law) then,

$$\tau = \frac{n}{2} \sigma_p \quad (5)$$

where σ_p is the particle stress. If particle fracture occurs when the stress in the particle reaches its ultimate tensile strength, $\sigma_{p,uts}$, then setting the boundary condition at

$$\sigma_p = \sigma_{p,\,uts} \quad (6)$$

and substituting into Eq.(5) gives a relationship between the strength of the particle and the interfacial shear stress such that if

$$\sigma_{p,uts} < \frac{2\tau}{n} \quad (7)$$

Then the particle will fracture. Similarly if interfacial debonding/yielding is considered to occur when the interfacial shear stress reaches its shear strength

$$\tau = \tau_{max} \quad (8)$$

Then by substituting Eq. (8) into Eq.(5) a boundary condition for particle/matrix interfacial fracture can be established whereby,

$$\tau_{max} < \frac{n\sigma_p}{2} \quad (9)$$

This approach suggests that the outcome of a matrix crack impinging on an embedded particle depends on the balance between the particle strength and the shear strength of the interface.

A linear stress–strain relation [14] at the macro level can be formulated as follows:

$$\bar{\sigma} = \bar{C}\bar{\varepsilon} \quad (10)$$

where $\bar{\sigma}$ is macro stress, and $\bar{\varepsilon}$ represents macro total strain and $\bar{C}$ and is macro stiffness matrix.

Table 1: Mechanical properties of AA2024 matrix and TiO_2 nanoparticles.

Property	AA2024	TiO_2
Density, g/cc	2.78	4.05
Elastic modulus, GPa	73.1	288
Ultimate tensile strength, MPa	395	368
Poisson's ratio	0.28	0.29
CTE, µm/m-^{o}C	21.1	11.8
Thermal Conductivity, W/m-K	121.0	11.8
Specific heat, J/kg-K	875	697

AA2024 alloy was used as a matrix material. The nanoparticulate was TiO_2 of average size 100nm. The material properties are given in table 1. The volume fractions of TiO_2 nanoparticulates were 10% and 30%. A square RVE (Fig. 1) was modeled to estimate the thermoelastic behavior AA2024/ TiO_2 nanoparticulate composites. The PLANE183 element was used to discretize the matrix and the nanoparticle. The interphase between TiO_2 nanoparticle and AA2024 alloy was discretized with CONTACT172 element. Both isothermal and hydrostatic pressure loads were applied all together on the RVE models.

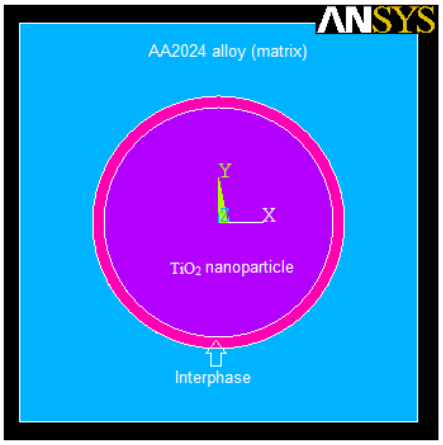

Fig. 1. The RVE model.

3. Results and Discussion

The finite element analysis (FEA) was carried out at 0oC to 300oC at constant pressure load on RVE models.

3.1 Micromechanics of thermo-elastic behavior

The strains along x- and y- directions of the applied load increased with increase in temperature (Fig. 2). The strains along the load direction (x) had a linear relationship with the temperature while the strains along transverse direction (y) of the applied load had a quadratic relationship with the temperature. The strains along y-direction were small due to low thermal conductivity of TiO_2 since the resultant strain is subtraction of elastic strains (compressive) from thermal strains along transverse direction.

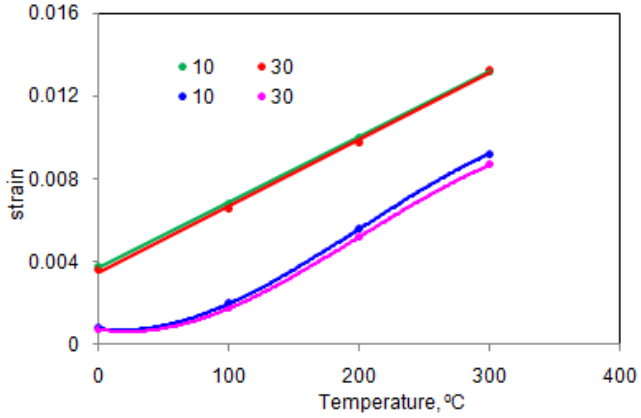

Fig. 2. Influence of temperature on thermoelastic strain.

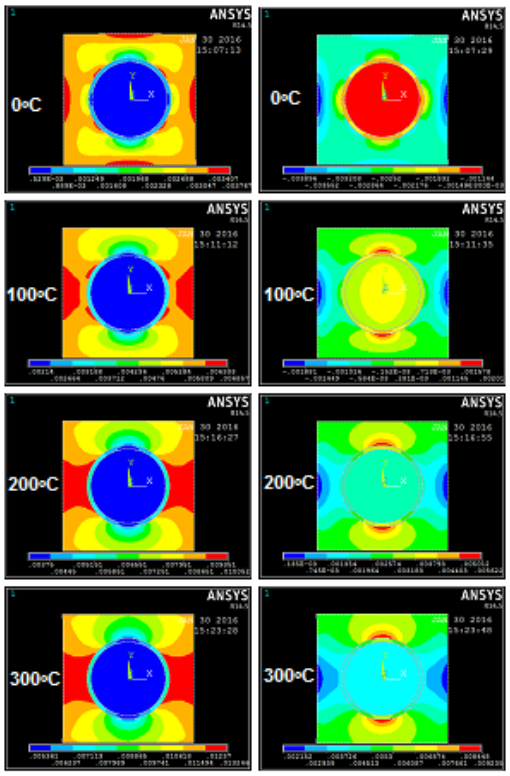

Fig. 3. Raster images of strains induced in AA1100/10%TiN composites.

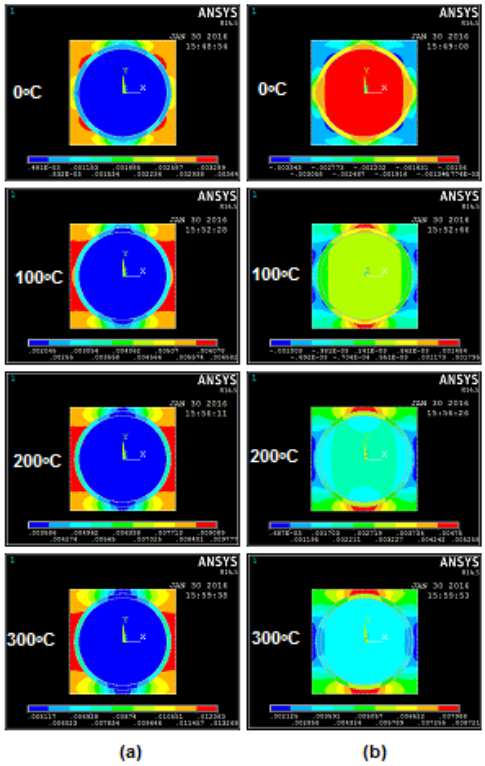

Fig. 4. Raster images of strains induced in AA1100/30% TiN composites.

For composites having 10% of TiO2 nanoparticles, the matrix AA2024 alloy had exhibited large strains along x-direction as the temperature changed from 0oC to 300oC temperature as showed in Fig. 3a. For composites having 10% of TiO2 nanoparticles, the interphase or near interphase of matrix alloy or nanoparticle had peeled large strains along y-direction as showed in Fig. 3b. The same kind of trend was observed with the composites comprising of 30% of TiO2 with marginally lower values of strains (Fig. 4).

The stresses along x- and y- directions increased with the temperature due to softening of nanocomposites as shown in Fig. 5. The stress induced along x-direction was higher than that induced along y-direction of hydrostatic pressure loading. This might be due to difference in coefficient of thermal expansion (CTE) and thermal conductivity of AA2024 alloy and TiO_2 nanoparticles [15, 16].

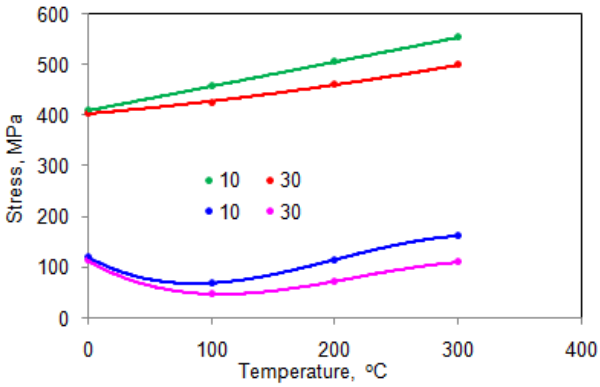

Figure 5: Influence of temperature on strength.

Figs. 6 and 7 show images of stresses derived from the finite element analysis. Very high stresses were induced either in TiO_2 nanoparticles or at the interphase. This is clear indication of load transfer from the AA2024 alloy to the TiO_2 nanoparticle as the temperature increased from 0oC to 300°C. The TiO_2 nanoparticles had undergone local stress variation as observed different color bands within them.

The tensile elastic modulus declined with the increase of temperature (Fig. 8). The elastic modulus was higher along x-direction (load direction) than that along transverse (y) direction of hydrostatic loading except at 0°C. The major Poisson's ratio increased with increase of temperature (Fig. 9). The major Poisson's ratio was higher for the composites comprising 30%Vp TiO_2 nanoparticulates than those having 10%Vp TiO_2 nanoparticulates. This is because of CTE and stiffness mismatch between AA2024 alloy matrix and TiO_2 nanoparticles.

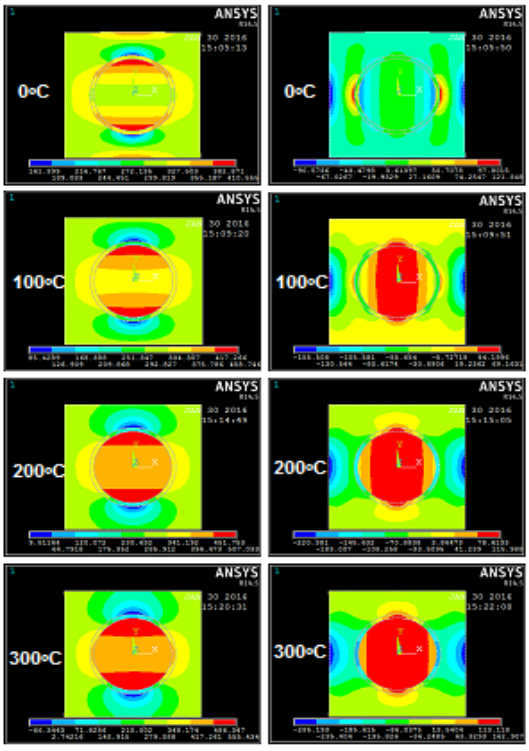

Fig. 6. Raster images of stresses induced in AA1100/10% TiN composites.

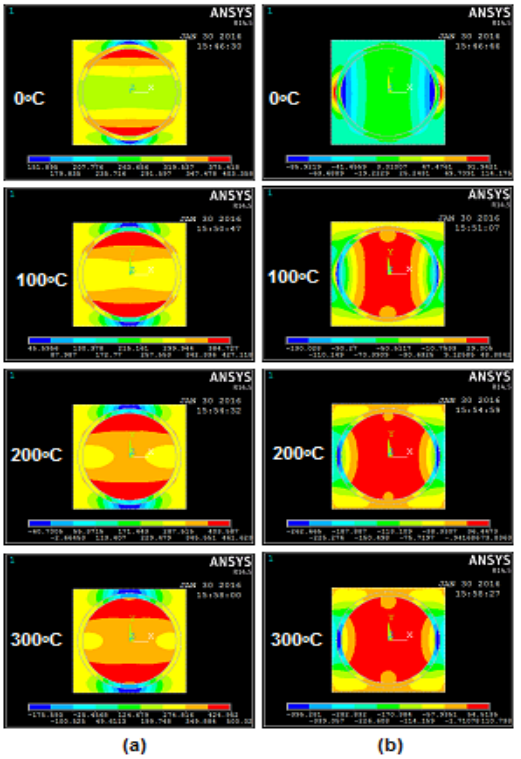

Fig. 7. Raster images of stresses induced in AA1100/30% TiN composites.

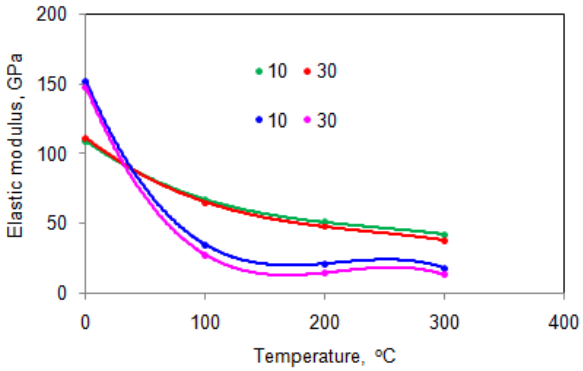

Fig. 8. Influence of temperature on elastic modulus: (a) Ex and (b) Ey.

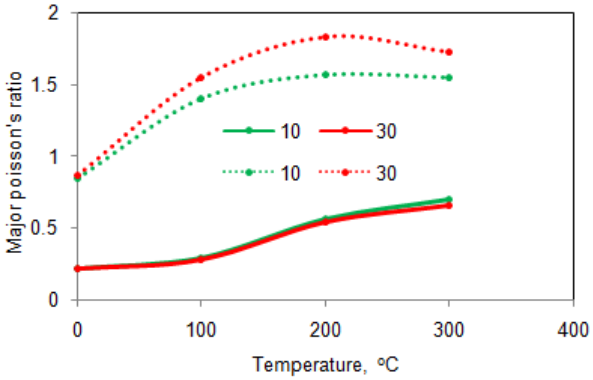

Fig. 9. Influence of temperature on major Poisson's ratio:

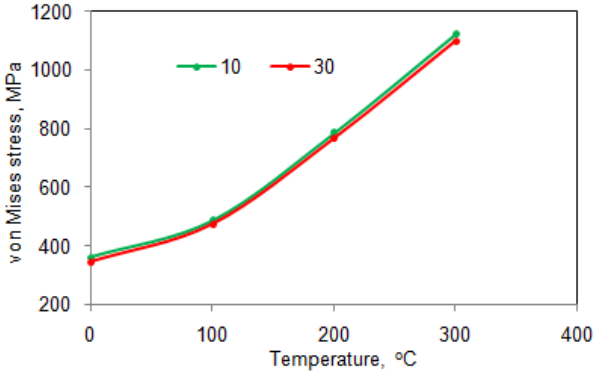

Fig. 10. Influence of temperature on von Mises stress.

3.2 Fracture behavior

The von Mises stress increased with the increase of temperature as a result of increased softening (Fig. 10). In all the composites, TiO_2 nanoparticles were fractured due to heavy transfer of load as shown in Fig. 11. The fracture of TiO_2 nanoparticles (A) and interphase (B) is revealed in scanning electron microscope (SEM) images (Fig. 12) of AA2024 alloy/30%TiO_2 exposed to 300oC. The local stress bands (C) were viewed in TiO2 nanoparticles.

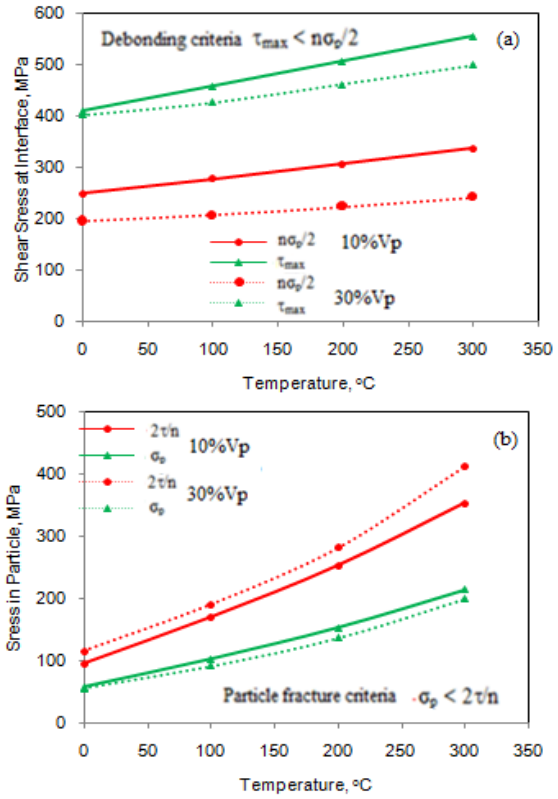

Fig. Failure criteria: (a) interface debonding and (b) Particulate facture.

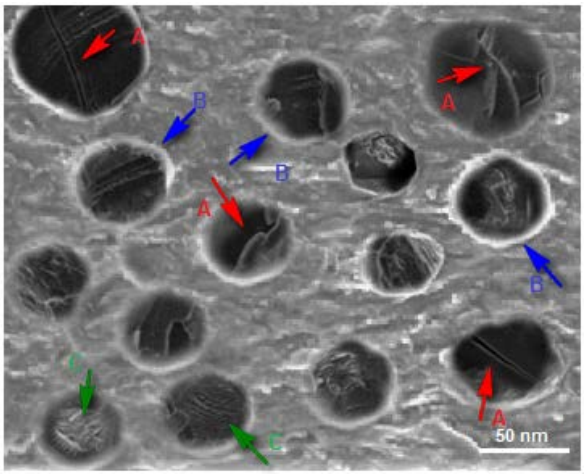

Fig. 12. SEM images illustrating rupture of interphase (A), stress or tear bands (B) and local stress bands (C) in nanoparticles. .

4. Conclusion

The thermoelastic strains and stresses induced in the AA2024 alloy/TiO2 nanocomposites were increased with the temperature. The elastic moduli decreased with increase of temperature. The rupture of TiO2 nanoparticle was occurred in the AA2024 alloy/TiO2 nanocomposites.

References

1. K.K. Chawla, Composite Materials: Science and Engineering, Springer-Verlag, 1998.
2. A. C. Reddy, B. Kotiveerchari and P. Rami Reddy, "Saving of Thermal Energy in Air-Gap Insulated Pistons Using Different Composite Materials for Crowns," International Journal of Scientific & Engineering Research, vol. 6, no. 3, 2015, pp. 71-74.
3. A. C. Reddy, "Tensile properties and fracture behavior of 6063/SiC_P metal matrix composites fabricated by investment casting process," International Journal of Mechanical Engineering and Materials Sciences, vol. 3, no. 1, 2010, pp.73-78.
4. A. C. Reddy, "Experimental Evaluation of Elastic Lattice Strains in the Discontinuously SiC Reinforced Al-alloy Composites," National Conference on Emerging Trends in Mechanical Engineering, Nagapur, 05-06th February, 2004.
5. M. Geni and M. Kikuchi, "Damage Analysis of Aluminum Matrix Composite Considering Non-uniform Distribution of SiC Particles," Acta Metallurgica, vol.46, no.9, 1998, pp.3125-3133.
6. A. C. Reddy and Essa Zitoun, "Matrix al-alloys for alumina particle reinforced metal matrix composites," Indian Foundry Journal, vol.55, no.1, 2009, pp.12-16.
7. A. C. Reddy and Essa Zitoun, "Tensile behavior 0f 6063/Al_2O_3 particulate metal matrix composites fabricated by investment casting process," International Journal of Applied Engineering Research, vol. 1, no.3, 2010, pp.542-552.
8. R. H. Pestes, S.V. Kamat, and J.P. Hirth, "Fracture toughness of Al-4%Mg/Al_2O_3 composites, Materials Science & Engineering," A: Structural Materials: Properties, Microstructure and Processing, vol.189A, 1994, pp. 9-14.
9. A. C. Reddy, "Studies on fracture behavior of brittle matrix and alumina trihydrate particulate composites," Indian Journal of Engineering & Materials Sciences, vol. 9, no. 5, 2002, pp.365-368.
10. A. C. Reddy, "Analysis of the Relationship Between the Interface Structure and the Strength of Carbon-Aluminum Composites," NATCON-ME, Bangalore, 13-14th March 2004
11. A. C. Reddy, "Interfacial Debonding Analysis in Terms of Interfacial Tractions for Titanium Boride/AA3003 Alloy Metal Matrix Composites," 1st National Conference on Modern Materials and Manufacturing, Pune, 19-20 December 1997.
12. A. C. Reddy, "Evaluation of Debonding and Dislocation Occurrences in Rhombus Silicon Nitride Particulate/AA4015 Alloy Metal Matrix Composites," 1st National Conference on Modern Materials and Manufacturing, Pune, 19-20 December 1997.

13. S. Suresh, A. Mortensen, and A. Needleman, "Fundamentals of MMCs," Butterworth- Heinemann Publishing Company, Stoneham, USA, 1993.
14. A. C. Reddy, "Influence of strain rate and temperature on superplastic behavior of sinter forged Al6061/SiC metal matrix composites," International Journal of Engineering Research & Technology, Vol.04, No.02, pp.189-198, 2011.
15. A. C. Reddy and B. Kotiveerachari, "Influence of microstructural changes caused by ageing on wear behaviour of Al6061/SiC composites," Journal of Metallurgy & Materials Science, Vol. 53, pp. 01, pp. 31-39, 2011.
16. N. I. Sax, Lewis, J. Richard, "Dangerous Properties of Industrial Materials III," New York, Van Nostrand Reinhold, 2000.